1D electromagnetic model reconstruction by modified inverse scattering series

Myoung Jae Kwon[1] & Roel Snieder[1]
[1] *Center for Wave Phenomena, Colorado School of Mines*

ABSTRACT

The inverse scattering series (ISS) is a tool that enables rapid interpretation of electromagnetic data using fewer computational resources and less a priori information than conventional approaches. However, the ISS converges only when the contrast between true and reference models is sufficiently small. We discuss the origin of the narrow range of convergence and qualitatively describe that there are two contradictory conditions that determine the convergence of the ISS. To mitigate the convergence conditions, we propose an alternative approach to electromagnetic data inversion: the modified inverse scattering series (MISS). The MISS is based on the iterative dissipative method (IDM), which provides an absolutely converging forward series. We consider several 1D models and study the applicability of the MISS to inverse problems of electromagnetic data in geophysics. The model tests reveal that compared to the ISS, the MISS converges for a wider contrast of the electric conductivity between true and reference models. The 1D tests also demonstrate that models reconstructed by the MISS are closer to true models than models generated via the ISS. This study shows that the MISS enables fast reconstruction of an electromagnetic model, which can be a good starting model for large-scale geophysical data processing, such as marine controlled-source electromagnetic (CSEM) data inversion.

Key words: Inverse scattering series (ISS), Modified inverse scattering series (MISS), Iterative dissipative method (IDM), Controlled-source electromagnetics (CSEM)

1 INTRODUCTION

Marine electromagnetic surveys are efficient complementary tools to seismic surveys in searching for a hydrocarbon reservoir (Hoversten *et al.*, 2006; Hu *et al.*, 2009; Kwon & Snieder, 2011). The advantage of electromagnetic exploration over seismic methods originates from its capability to discern the reservoir composition: hydrocarbon is a poor electric conductor while water within a reservoir increases the electric conductivity. The most well-known marine electromagnetic technique for hydrocarbon exploration is the controlled-source electromagnetic (CSEM) method (Chave & Cox, 1982; Cox *et al.*, 1986; Srnka *et al.*, 2006). The typical frequency range and depth of investigation of the method are 0.1 - 10 Hz and several kilometers, respectively. To ensure greater depth penetration, CSEM data can be combined with magnetotelluric (MT) data, which are generated by natural low-frequency sources (Abubakar *et al.*, 2009; Commer & Newman, 2009).

There is a wide spectrum of approaches to the modeling of CSEM and MT data: the finite-difference (Yee, 1966; Alumbaugh *et al.*, 1996), finite-element (Pridmore *et al.*, 1981; Um *et al.*, 2010), and integral equation methods (Hohmann, 1975; Zhdanov *et al.*, 2006). Several approximate methods that require various prerequisites such as a low-contrast assumption (Habashy *et al.*, 1993; Torres-Verdín & Habashy, 2001) are also available. Among them, the finite-difference method is the most prevalent approach for large-scale geophysical problems because of its apparent simplicity of numerical implementation and adaptability to model complexity. The

finite-difference method, on the other hand, necessitates more computational resources and processing time. Furthermore, a reasonable interpretation of marine electromagnetic surveys generally involves 3D inversion, which still remains a difficult and computationally intense task (Newman & Alumbaugh, 1997; Commer & Newman, 2008). Only recently, the first successful examples of 3D electromagnetic inversion have been reported, and the inverse problem is currently an area of intense research (Avdeev, 2005).

The difficulty of 3D electromagnetic inversion arises from the fact that the inverse problem is large-scale, strongly nonlinear, and severely ill-posed (Jackson, 1972; Parker, 1977). The inversion process aims to retrieve a model that has infinitely many degrees of freedom from a finite amount of data (Snieder, 1998). There are many factors that help constrain the output from the process that include the use of a priori information, using different starting models of the inversion, and the design of the data misfit function or model regularization (Tikhonov & Arsenin, 1977). In this study, we implement a scheme for electromagnetic data processing that enables rapid interpretation of data and provides a good starting model for more rigorous large-scale inversion. The inverse scattering series (ISS) is adequate for this goal because it can effectively resolve the nonlinearity of an inverse problem and reconstruct an electromagnetic model using fewer computational resources and less a priori information than the conventional approaches addressed above.

The inverse scattering theory quantitatively retrieves the scatterers from knowledge of the scattering data. The theory originates from inverse problems in quantum scattering theory and formal solutions of inverse scattering problems (Gel'fand & Levitan, 1951; Jost & Kohn, 1952; Moses, 1956; Prosser, 1969). The ISS expresses the retrieved model perturbation as a series in order of the scattered field. The geophysical application of the ISS has focused on seismic exploration, in particular on multiple suppressions (Weglein *et al.*, 1997) and seismic imaging (Weglein *et al.*, 2010). However the ISS has not been widely applied to the interpretation of electromagnetic surveys. Kwon and Snieder (2010) have recently investigated the feasibility of this application and clarified the difference between scattering series for acoustic wave propagation and electromagnetic diffusion. Their analytic study also identifies convergence conditions of the forward and inverse series for homogeneous models.

In the following, we formulate the ISS for 1D electromagnetic model reconstruction and exemplify that the ISS converges only when the contrast between the true and reference models is sufficiently small. We also show that in addition to the convergence condition of the inverse series, there is another condition that determines the convergence/divergence of the ISS, and we illustrate that this condition is closely related to the convergence condition of the forward series. We thereafter propose an alternative approach, the modified inverse scattering series (MISS). The MISS is based on the iterative dissipative method (IDM), which guarantees an absolutely converging forward series (Singer, 1995; Singer & Fainberg, 1995; Pankratov *et al.*, 1995), and the convergence of the MISS is thus free from the newly identified condition. Finally, we show that the MISS more robustly converges than the ISS and discuss the advantage of the MISS over the original by comparing the inversion results from the two methods.

2 1D FORMULATION OF INVERSE SCATTERING SERIES

The fundamental equations for electromagnetism, the Maxwell's equations (Jackson, 1999), in an isotropic medium are

$$\nabla \times \mathbf{E} - i\omega\mu\mathbf{H} = 0, \tag{1}$$

$$\nabla \times \mathbf{H} - (\sigma - i\omega\epsilon)\,\mathbf{E} = \mathbf{J}_s, \tag{2}$$

where $\mathbf{E}$ is the electric field (V/m), $\mathbf{H}$ the magnetic field (A/m), $\mathbf{J}_s$ the electric current source (A/m^2), μ the magnetic permeability (N/A^2), σ the electric conductivity (S/m), and ϵ the dielectric permittivity (C^2/Nm^2), respectively. We consider a single Fourier component corresponding to a time variation $e^{-i\omega t}$. Outside of certain types of ore bodies, magnetizable materials are rare in the subsurface (Chave & Cox, 1982), and we take the magnetic permeability μ to be the free space value. For frequencies of electromagnetic methods used in hydrocarbon exploration, the displacement current ($\omega\epsilon\mathbf{E}$) is much smaller than the induction current ($\sigma\mathbf{E}$) in the subsurface (Hohmann, 1975). We therefore ignore the variation of the dielectric permittivity ϵ and approximate it to the value of water. The 1D electromagnetic model of this study is illustrated in Figure 1: the electric conductivity varies in the z-axis direction, and a harmonic plane wave propagates in the same direction. Applying the 1D assumption to the Maxwell's equations, we derive the following scalar Helmholtz equation:

$$L(z;\omega)\,G(z,z_s;\omega) = -\delta(z - z_s), \tag{3}$$

where G is the Green function of the electric field (the component of $\mathbf{E}$ parallel to the electric current source), z_s represents the location of the unit current source, and the differential operator L is

$$L(z;\omega) = \frac{1}{i\omega\mu}\frac{d^2}{dz^2} + \sigma(z) - i\omega\epsilon. \tag{4}$$

Note that as shown in Figure 1, the electric field direction is opposite to the electric current source, and the unit of the Green function is Ω (electric field / (unit current source × unit length)).

We consider two types of 1D electromagnetic media: the true (perturbed) and reference (unperturbed)

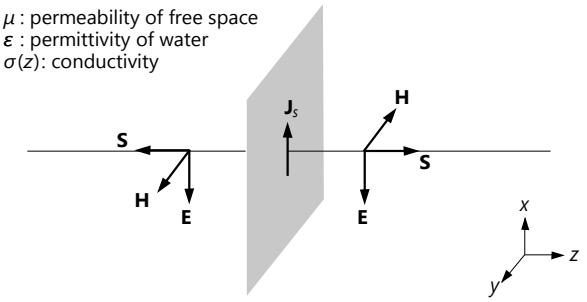

Figure 1. 1D electromagnetic radiation geometry for this study. The Poynting vector **S** indicates the direction of energy flux. The electric field **E** is divergenceless, and the direction of the electric field is opposite to that of the infinitely planar current source $\mathbf{J}_s$ on the (x, y) plane. The electric conductivity σ varies in the direction normal to the current source.

media. The governing equations for the two media are represented by two differential operators: L and L_0, respectively. We denote the Green functions for the two media as G and G_0, respectively. The Lippmann-Schwinger equation (Lippmann & Schwinger, 1950; Colton & Kress, 1998) relates the Green functions for the true and reference models as

$$G(z, z_s; \omega) = G_0(z, z_s; \omega) + \int G_0(z, z'; \omega)\, P(z')\, G(z', z_s; \omega)\, dz', \tag{5}$$

where the perturbation P is defined as the difference between the two differential operators:

$$P(z) = L(z; \omega) - L_0(z; \omega) = \sigma(z) - \sigma_0(z). \tag{6}$$

The scattered field G^s is the difference between the two Green functions $(G - G_0)$ that can, in operator form, be expanded as an infinite series in order of the perturbation P:

$$G^s = G_0 P G_0 + G_0 P G_0 P G_0 + \cdots. \tag{7}$$

The above equation is known as the Born, Neumann, or forward scattering series (Weglein *et al.*, 1997). It is known that for homogeneous models, the forward scattering series of electromagnetic diffusion problems converges only when the reference medium is sufficiently conductive (Kwon & Snieder, 2010) such that

$$\sigma < 2\,\sigma_0. \tag{8}$$

The divergence of the forward series implies that strong scattering occurs, and the term $G_0 P$ in equation (5) is no longer a contracting kernel (Pankratov *et al.*, 1995).

While the forward series describes the scattered field G^s as a series in order of the perturbation P, the inverse scattering series (ISS) addresses the perturbation as a series expansion in order of the scattered field:

$$P = P_1 + P_2 + P_3 + \cdots, \tag{9}$$

where P_n is the portion of P that is of the nth order of the scattered field. Substituting expression (9) into the forward series (equation (7)) and equating terms that are of the same order of the scattered field G^s (Prosser, 1969; Weglein *et al.*, 2003) yield the following set of integral equations represented in operator form:

$$\begin{aligned} G^s &= G_0 P_1 G_0, & (10)\\ 0 &= G_0 P_2 G_0 + G_0 P_1 G_0 P_1 G_0, & (11)\\ 0 &= G_0 P_3 G_0 + G_0 P_1 G_0 P_2 G_0 + G_0 P_2 G_0 P_1 G_0 \\ &\quad + G_0 P_1 G_0 P_1 G_0 P_1 G_0, & (12)\\ &\quad \cdots \end{aligned}$$

Equation (10) is the linear or Born approximation which allows P_1 to be determined from the scattered field G^s. P_2 is then computed from P_1 with equation (11). Equation (12) determines P_3 from P_1 and P_2. Starting with the scattered field, one continues the iterative process and constructs the entire series for the perturbation P. The nth order term in the inverse series is derived by solving the following Fredholm integral equation of the first kind (Morse & Feshbach, 1953):

$$D_n(G^s, P_1, P_2, \cdots, P_{n-1}; \omega) = \int G_0(z, z'; \omega)\, P_n(z')\, G_0(z', z_s; \omega)\, dz', \tag{13}$$

where D_n generally consists of $2^{n-1} - 1$ terms. In this study, we assume that the source and receiver are coincident. Applying this assumption and utilizing the reciprocity principle yield the following relation:

$$G_0 P_l G_0 P_m G_0 = G_0 P_m G_0 P_l G_0, \tag{14}$$

where l and m are arbitrary. The above relation simplifies D_n to

$$D_n = \begin{cases} G^s & (n = 1), \\ -G_0 P_1 G_0 P_1 G_0 & (n = 2), \\ -G_0 P_1 D_{n-1} & (n = 3, 4, \cdots). \end{cases} \tag{15}$$

Kwon and Snieder (2010) have shown that for homogeneous models, expression (9) converges only for weakly scattered fields that satisfy

$$\left| \frac{G^s}{G_0} \right| < 1. \tag{16}$$

This convergence condition suggests that for electromagnetic diffusion, we can improve the convergence of the ISS by choosing a resistive reference medium for which the amplitude of the reference Green function $|G_0|$ is large.

The main advantage of the ISS is that it enables rapid interpretation of electromagnetic data. The merit of the ISS is best taken advantage of by choosing a reference model for which the Green function G_0 is known analytically. Throughout this study, we assume the simplest reference model, a homogeneous medium. In the case of a homogeneous reference medium, the solution of equation (3) is (Morse & Feshbach, 1953)

$$G_0(z, z_s; \omega) = -\frac{\omega\mu}{2k_0} e^{ik_0|z - z_s|}, \tag{17}$$

where $k_0^2 = \omega^2\mu\epsilon + i\omega\mu\sigma_0$, and equation (13) becomes

$$D_n(\omega) = \left(\frac{\omega\mu}{2k_0}\right)^2 \int e^{ik_0(|z-z'|+|z'-z_s|)} P_n(z')\, dz'. \tag{18}$$

The above expression can, however, generate a negative conductivity. A conventional approach to avoid this unphysical solution is inverting for the logarithm of the electric conductivity (Newman & Alumbaugh, 1997). Following that convention, we introduce an intermediate parameter M such that $\sigma = \sigma_0\, e^M$, assume that σ is close to the reference conductivity, and approximate the perturbation as

$$P(z) = \sigma(z) - \sigma_0 \simeq \sigma_0\, M(z). \tag{19}$$

Expression (18) is then rewritten as

$$D_n(\omega) = \left(\frac{\omega\mu}{2k_0}\right)^2 \int \sigma_0 e^{ik_0(|z-z'|+|z'-z_s|)} M_n(z')\, dz'. \tag{20}$$

We solve equation (20) for M_n through singular value decomposition (Golub & Reinsch, 1970) and reconstruct the electric conductivity as follows:

$$\sigma(z) = \sigma_0 \exp\left(\sum M_n(z)\right). \tag{21}$$

Note that the approximation in equations (19) - (21) is a deviation from the rigorous definition of the ISS approach in equations (6) - (18) because expression (19) is a linear approximation, and we discard higher order terms of the Taylor series expansion of $\sigma(M)$. We adopt the approximation to clarify limitations of the ISS and to highlight the advantages of a modified approach that we propose later in this study.

3 MODEL TESTS OF INVERSE SCATTERING SERIES

To simulate the electric field for true (perturbed) models, we use the finite-difference method with the staggered grid algorithm (Yee, 1966) and suppress artificial reflections from the boundary of the modeling domain via the perfectly match layer method (Berenger, 1994). The spatial range of the modeling domain is $-20 < z < 20$ km, the spatial discretization interval Δz is 20 m, and the unit electric current source is at the origin. We add frequency independent Gaussian random noise with a standard deviation 10^{-9} V/m to the simulated electric field. To solve equation (20) for M_n, we discretize the inverse problem: the frequency sampling range is 0.1 - 10 Hz, and 51 frequency samples are evenly distributed on a logarithmic scale.

The inverse problem is ill-posed (Jackson, 1972; Parker, 1977) and nonlinear (Snieder, 1998). It is thus necessary to include a stabilizing functional (Tikhonov & Arsenin, 1977) for the reconstruction of a stable solution. The stabilizing functional Φ_m is part of a penalty functional Φ and trades off between data misfit Φ_d and a priori information: $\Phi = \Phi_d + \beta\Phi_m$, where β is a trade-off coefficient or model regularization factor. The choice of stabilizing functional is important for electromagnetic inverse problems. In this study, we regularize the roughness of the model (Constable *et al.*, 1987) as follows:

$$\Phi_m = \int \left(w(z)\, \frac{d^2M}{dz^2}\right)^2 dz, \tag{22}$$

where a depth weighting factor $w(z)$ is proportional to $e^{|z/1\mathrm{km}|}$. The trade-off coefficient β is model-dependent, and we determine the coefficient from an L-curve analysis (Hansen, 1992) for each model. In this section, we consider resistive and conductive anomaly models.

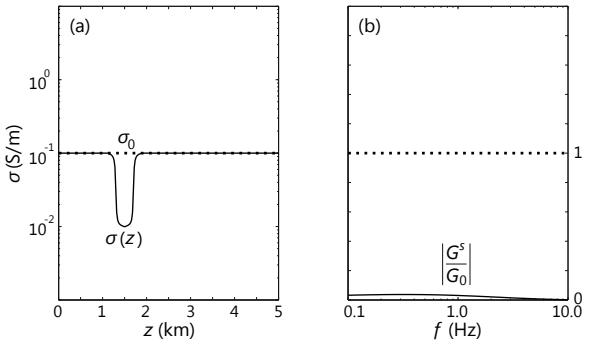

Figure 2. Resistive anomaly model. (a) True model (solid curve) versus reference model (dotted line) of the inverse series. The reference conductivity is identical with the background conductivity of the true model. (b) The convergence requirement of the inverse series, expression (16), is satisfied in the employed frequency range.

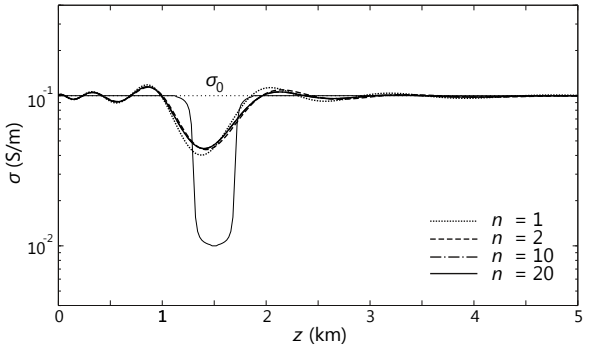

Figure 3. ISS solutions for the resistive anomaly model shown in Figure 2. The solutions are derived from equation (21) and compared for increasing order n of the inverse series. The thin solid curve denotes the true model. The ISS converges.

3.1 Resistive anomaly model

Figure 2(a) presents the true (solid curve) and reference (dotted line) media of the resistive anomaly model. The

true medium consists of a resistive structure at $z = 1.5$ km and a conductive background. Note that the resistive layer constitutes a strong perturbation: the ratio of the electric conductivity between the conductive background and resistive target is 10. The conductivity of the background is same as that of the reference medium. Figure 2(b) illustrates that within the frequency range used in the experiment, the scattered field has a smaller amplitude than the reference Green function and fulfills the convergence condition of the inverse series in expression (16).

Figure 3 demonstrates how the ISS evolves as we include higher order perturbation terms. The inverse series converges for the resistive anomaly model: the ISS solution evaluated up to the 10th order ($n = 10$) is practically identical to the solution evaluated up to the 20th order ($n = 20$). This convergence pattern of the ISS is consistent with the value of $|G^s/G_0|$ shown in Figure 2(b). The reconstructed model is a linear combination of singular vectors that span the resolvable model space and shows a more significant oscillatory variation near the resistive target. The reconstructed conductivity value of the resistive target is roughly three times that of the true model because the reconstruction of the resistive target is physically limited by the relatively conductive background medium, which shields the resistive structure. The Born approximation ($n = 1$) accounts for most of reconstructing the resistive structure of this model.

3.2 Conductive anomaly model

Figure 4 depicts a conductive structure at $z = 1.5$ km and a relatively resistive background. The conductivity of the reference model is same as that of the background medium. As in the case of the previous model, the scattered field has a smaller amplitude than the reference Green function within the employed frequency range, which suggests convergence of the inverse series. The inverse series shown in Figure 5, however, does not converge for the conductive anomaly model. The model reconstructed by the Born approximation (dotted curve) reveals the conductive structure, but the subsequent higher order solutions diverge. The divergence of the ISS for this model suggests that in addition to the amplitude of the scattered field G^s (expression (16)), there is another factor that affects the convergence/divergence of the ISS. Recall that during the ISS procedure, we iteratively solve equation (20) for the increasing order n of the inverse series, and its solution M_n depends on the left hand side of equation (20), D_n. Figure 6 shows that contrary to the case of the resistive anomaly model, $|D_n|$ increases exponentially during the iterative process for the conductive anomaly model. This divergence of D_n causes the divergence of the ISS.

To illustrate the convergence condition of D_n, we

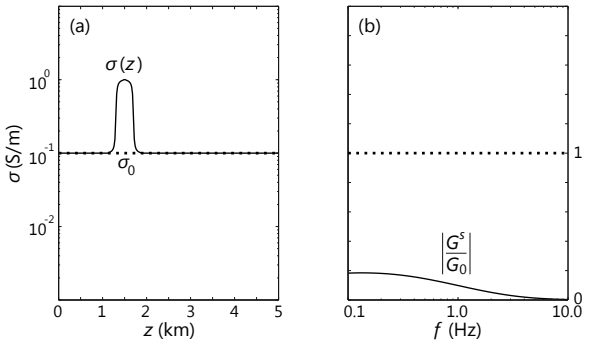

Figure 4. Conductive anomaly model. (a) True model (solid curve) versus reference model (dotted line) of the inverse series. The reference conductivity is identical with the background conductivity of the true model. (b) The convergence requirement of the inverse series, expression (16), is satisfied in the employed frequency range.

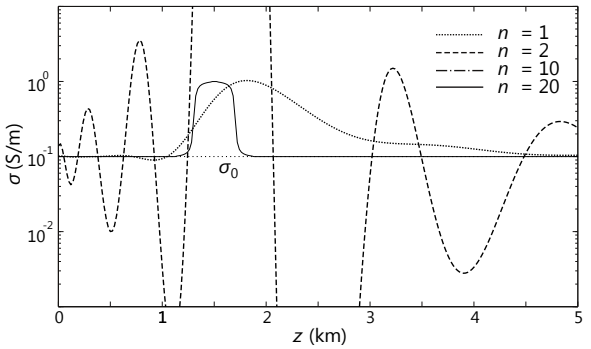

Figure 5. ISS solutions for the conductive anomaly model shown in Figure 4. The solutions are derived from equation (21) and compared for increasing order n of the inverse series. The thin solid curve denotes the true model. The ISS diverges. The ISS solutions evaluated up to the 10th and 20th orders are not displayed because of the rapid divergence.

rewrite D_n from equation (15) as

$$D_n = (-1)^{n+1} (G_0 P_1)^n G_0 \tag{23}$$

and observe the similarity between D_n and the forward scattering series. Assume that we solve a forward scattering problem for a true model that is identical to the model recovered from the Born approximation ($P = P_1$ and $\sigma = \sigma_1$). The nth order term in this forward series then becomes

$$G_n^s = (G_0 P_1)^n G_0. \tag{24}$$

Considering the convergence condition for homogeneous models in equation (8), we qualitatively estimate the convergence condition of this forward series as

$$\sigma_1 < 2\,\sigma_0. \tag{25}$$

Note that equations (23) and (24) have an identical kernel $G_0 P_1$, and expression (25) therefore also qualitatively describes the convergence condition of D_n: for

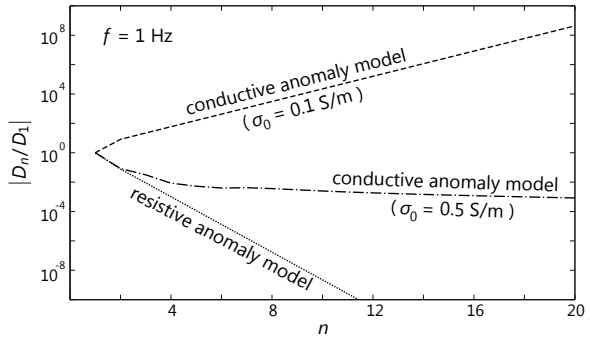

Figure 6. The left hand side of equation (20), D_n, as a function of the order n of the ISS for $f = 1$ Hz. The dotted and dashed curves represent the ratio $|D_n/D_1|$ for the models shown in Figures 2 and 4, respectively. Contrary to the resistive anomaly model, the ratio exhibits an exponential increase for the conductive anomaly model with $\sigma_0 = 0.1$ S/m. This exponential increase causes the divergence of the ISS (Figure 5). Choosing a more conductive reference model ($\sigma_0 = 0.5$ S/m) decreases the ratio (dot-dashed curve).

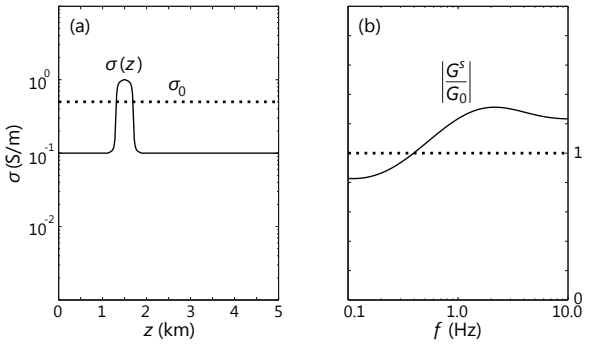

Figure 7. Conductive anomaly model with a more conductive reference model than the model shown in Figure 4. (a) True model (solid curve) versus reference model (dotted line) of the inverse series. The reference conductivity is 5 times larger than the background conductivity of the actual medium. (b) The convergence requirement of the inverse series, expression (16), is violated in the employed frequency range.

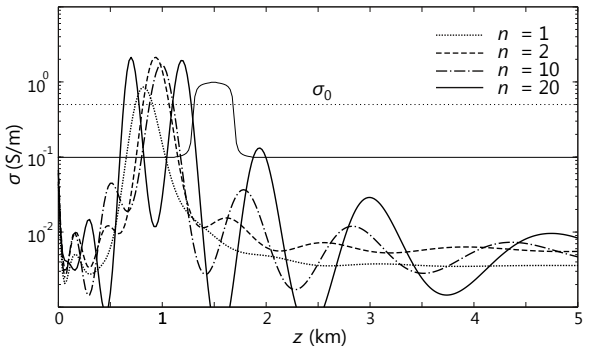

Figure 8. ISS solutions for the conductive anomaly model shown in Figure 7. The solutions are derived from equation (21) and compared for increasing order n of the inverse series. The thin solid curve denotes the true model. The ISS diverges.

the convergence of D_n, the reconstructed model from the Born approximation σ_1 needs to be sufficiently resistive compared to the reference model. In other words, it is necessary to choose a sufficiently conductive reference model that allows σ_1 to satisfy expression (25).

Figure 5 shows that near $z = 1.7$ km, the maximum conductivity of the solution retrieved from the Born approximation ($n = 1$) is 10 times larger than the reference conductivity (0.1 S/m), and the criterion (25) for convergence is not satisfied. The left hand side of equation (20) and the inverse series consequently diverge as we incorporate higher order terms. This example demonstrates the challenge of reconstructing a conductive anomaly via the inverse scattering formulation and suggests that for the convergence of the inverse series, the reference model must be sufficiently conductive such that the Born approximation yields a solution that satisfies expression (25). One therefore may choose a more conductive reference model that allows D_n to decrease during the ISS procedure as shown in Figure 6 (dot-dashed curve). Figure 7(a) presents the situation, where the reference conductivity σ_0 is 5 times larger than the background value of the previous example in Figure4(a). The more conductive reference model yields, however, a smaller amplitude of the reference Green function and a larger ratio between the scattered field and reference Green function in expression (16). Figure 7(b) shows that by choosing the more conductive reference model, the convergence condition of the inverse series ($|G^s/G_0| < 1$) is violated. The corresponding divergence of the inverse series is demonstrated in Figure 8.

3.3 Limitation of inverse scattering series

The convergence conditions of expressions (16) and (25) are contradictory: expression (16) favors more a resistive reference model, and expression (25) prefers more a conductive model. The two examples presented in Figures 4 - 8 pose the dilemma of choosing a reference model, which is inherent in the ISS procedure. Figure 9 summarizes the dilemma. As we choose a more conductive reference model, it is increasingly likely to violate the convergence condition of the inverse series in expression (16). On the other hand, the left hand side of equation (20) more readily diverges by choosing a more resistive reference model. The two contradictory conditions result in a narrow range of the reference model in which the ISS converges. This limitation of the ISS therefore necessitates an alternative approach of the inverse series. In this study, we remove the lower bound of con-

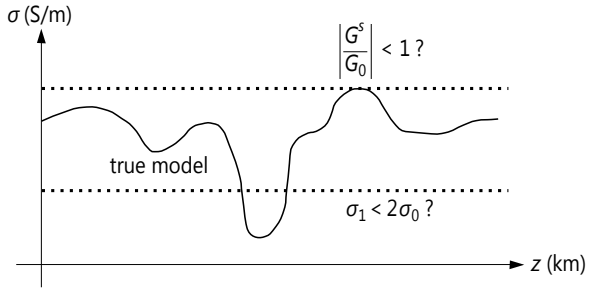

Figure 9. Dilemma of the ISS. A conductive reference model increases the possibility of violating the convergence condition of inverse series, expression (16). A resistive reference model, on the other hand, can result in the divergence of the left hand side of equation (20) and the inverse series itself. The range of the reference conductivity that allows convergence of the inverse series is limited by both the upper and lower bounds (dotted lines).

vergence in Figure 9 and guarantee the convergence of the inverse series within a wider range of reference models.

4 1D FORMULATION OF MODIFIED INVERSE SCATTERING SERIES

As discussed in the previous section, the application of the ISS is limited by both the convergence condition of the inverse series and that of D_n, which is closely related to the forward series. We next remove the latter limitation. For electromagnetic diffusion, the iterative dissipative method (IDM) allows one to formulate an absolutely converging forward series for physically meaningful medium parameters, i.e., positive and finite electric conductivity. The IDM is also an efficient preconditioner that is necessary for large scale 3D electromagnetic forward problems (Avdeev, 2005). The IDM has been implemented for 3D electromagnetic problems (Avdeev *et al.*, 1997) and applied to forward simulations of field data (Kuvshinov *et al.*, 2005). In this study, we apply the IDM in an inverse sense and formulate an alternative approach of the inverse series: the modified inverse scattering series (MISS). The application of the modified approach is not restricted by the convergence condition of the forward series.

The basic idea of the IDM originates from the fact that the electric current created in a conductive medium by an external current source is smaller than the external current. The IDM is valid for arbitrary conductive media (Singer, 1995; Singer & Fainberg, 1995). The IDM transforms the Lippmann-Schwinger equation (5) into the following modified scattering equation (Avdeev *et al.*, 2002):

$$\chi(z,z_s;\omega) = \chi_0(z,z_s;\omega) + \int Q(z,z';\omega)\,R(z')\,\chi(z',z_s;\omega)\,dz', \tag{26}$$

where

$$\chi(z,z_s;\omega) = \frac{1}{2\sqrt{\sigma_0(z)}}\big[\,(\sigma(z)+\sigma_0(z))\,G(z,z_s;\omega) - 2\sigma_0(z)\,G_0(z,z_s;\omega)\,\big], \tag{27}$$

$$\chi_0(z,z_s;\omega) = \int Q(z,z';\omega)\sqrt{\sigma_0(z')}\,R(z')G_0(z',z_s;\omega)\,dz', \tag{28}$$

$$Q(z,z';\omega) = \delta(z-z') + 2\sqrt{\sigma_0(z)}\;G_0(z,z';\omega)\;\sqrt{\sigma_0(z')}, \tag{29}$$

and the conductivity ratio R is defined as

$$-1 \;<\; R(z) = \frac{\sigma(z)-\sigma_0(z)}{\sigma(z)+\sigma_0(z)} \;<\; 1. \tag{30}$$

Contrary to the Lippmann-Schwinger equation, the modified scattering equation has a contracting kernel QR such that

$$\forall\chi: \quad \left\| \int Q(z,z';\omega)\,R(z')\,\chi(z',z_s;\omega)\,dz' \right\| \;<\; \|\chi\|, \tag{31}$$

where $\|\chi\|$ denotes the L_2-norm of χ (Pankratov *et al.*, 1995). Equation (26) therefore yields the following forward series that absolutely converges:

$$\chi = \chi_0 + QR\chi_0 + QRQR\chi_0 + \cdots. \tag{32}$$

In this modified forward series, the χ field is expressed as a series in order of the conductivity ratio R, and the true Green function G is subsequently derived using equation (27) from the χ field and electric conductivity at the receiver location.

In this study, we consider homogeneous reference models and rewrite equation (32) as

$$\frac{\chi}{\sqrt{\sigma_0}} = QRG_0 + QRQRG_0 + \cdots. \tag{33}$$

Following the procedure of the ISS presented in the previous section, we formulate the MISS that describes the conductivity ratio R as a series in order of the χ field:

$$R = R_1 + R_2 + R_3 + \cdots, \tag{34}$$

where R_n is the portion of R that is of the nth order of the χ field. We substitute the above series into equation (33), equate terms that are of the same order of the χ field, and derive the following integral equation:

$$\tilde{D}_n(\chi,R_1,R_2,\cdots,R_{n-1};\omega) = \int Q(z,z';\omega)\,R_n(z')\,G_0(z',z_s;\omega)\,dz', \tag{35}$$

which allows one to iteratively solve for R_n from the measured χ field and all of the lower order terms of the modified inverse series. Note that for the evaluation of the χ field, we require both the electric conductivity at

the receiver location and the scattered field (equation (27)). As in the case of the ISS, $\tilde{D}_n$ consists of $2^{n-1}-1$ terms for higher order cases. In this study, we locate the source and receiver at the same position ($z=0$), assume that the reference conductivity at the location is the true electric conductivity, and establish the following relation in operator form:

$$QR_lQR_mG_0 = QR_mQR_lG_0, \tag{36}$$

where l and m are arbitrary. The above relation simplifies $\tilde{D}_n$ to

$$\tilde{D}_n = \begin{cases} \chi/\sqrt{\sigma_0} & (n=1), \\ -QR_1QR_1G_0 & (n=2), \\ -QR_1\tilde{D}_{n-1} & (n=3,4,\cdots). \end{cases} \tag{37}$$

Since QR_1 is a contracting kernel, $\tilde{D}_n$ does not diverge. The convergence of $\tilde{D}_n$ implies that we resolve the dilemma of the ISS and remove the lower limit of convergence in Figure 9. The reference Green function is given by equation (17), and equation (35) is expressed as

$$\begin{aligned} \tilde{D}_n(\omega) &= R_n(z)\, G_0(z,z_s;\omega) \\ &\quad + \int G_0(z,z';\omega)\, R_n(z')\, G_0(z',z_s;\omega)\, dz' \\ &= \left(\frac{\omega\mu}{2k_0}\right)^2 \int 2\sigma_0 e^{ik_0(|z-z'|+|z'-z_s|)} R_n(z')\, dz', \end{aligned} \tag{38}$$

where we apply that the reference conductivity is the true electric conductivity at the receiver location ($R_n(z)=0$). Note the similarity between the equation above and equation (20). We iteratively solve equations (37) and (38) for R_n and reconstruct the electric conductivity from

$$\sigma(z) = \sigma_0 \frac{1+\sum R_n(z)}{1-\sum R_n(z)}. \tag{39}$$

5 MODEL TESTS OF MODIFIED INVERSE SCATTERING SERIES

In this section, we identify a different convergence pattern between the ISS and MISS for three representative models: resistive, conductive, and complex anomaly models. We also discuss the difference between the inversion results from the ISS and MISS. The input electric field data are identical for the two cases. The stabilizing functional Φ_m however is not identical. As shown in equation (22), the implemented ISS approach recovers models that exhibit a smooth variation in terms of the logarithm of the electric conductivity. The MISS, on the other hand, regularize the conductivity ratio R as

$$\Phi_m = \int \left(w(z) \frac{d^2R}{dz^2} \right)^2 dz, \tag{40}$$

where $w(z)$ is the same depth weighting factor as the ISS. Therefore, the trade-off coefficient β should be different from the model tests of the ISS, and we derive the model-dependent coefficient from an independent L-curve analysis. We also require the trade-off coefficient to yield a physically valid electric conductivity: $-1 < R < 1$. The rest of the MISS procedure is identical to that of the ISS procedure.

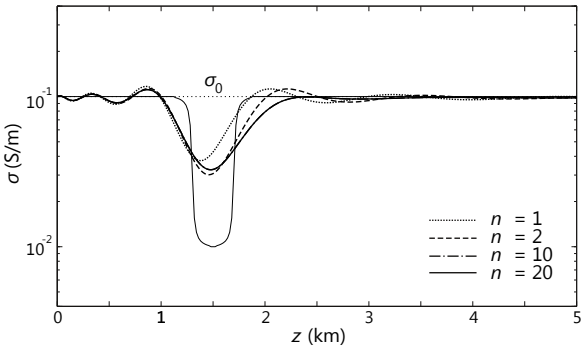

Figure 10. MISS solutions for the resistive anomaly model shown in Figure 2. The solutions are derived from equation (39) and compared for increasing order n of the inverse series. The thin solid curve denotes the true model. Both the ISS (Figure 3) and MISS converge.

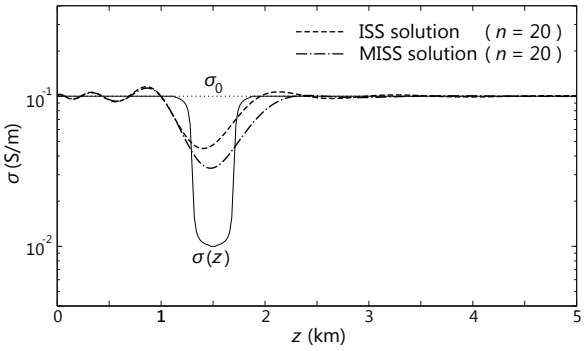

Figure 11. Comparison between the reconstructed models from the ISS and MISS for the resistive anomaly model shown in Figure 2. The MISS solution (dot-dashed curve) is closer to the true model (thin solid curve) than the model generated via the ISS (dashed curve).

5.1 Resistive anomaly model

We consider the model of Figures 2 and 3. Figure 10 shows that as in the case of the ISS, the MISS converges for the resistive anomaly model. The convergence criterion illustrated in Figure 2(b) adequately predicts the convergence of the modified inverse series. The convergence pattern also shows that the Born approximation ($n=1$) contributes most to the model reconstruction of this resistive structure, and the contribution of the higher order terms are less significant.

Figure 11 compares the two solutions from the ISS and MISS. The difference between the two inversion results are insignificant near the origin and becomes more

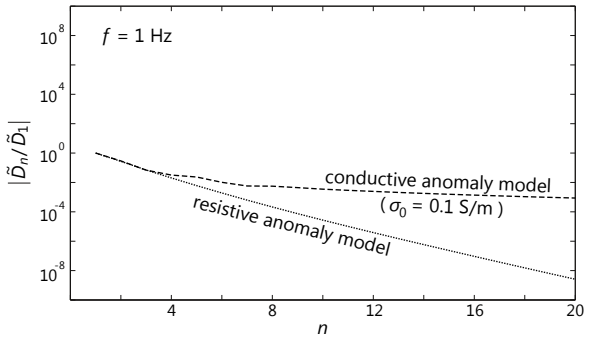

Figure 12. The left hand side of equation (38), $\tilde{D}_n$, as a function of the order n of the MISS for $f = 1$ Hz. The dotted and dashed curves represent the ratio $|\tilde{D}_n/\tilde{D}_1|$ for the models shown in Figures 2 and 4, respectively. Contrary to the case of the ISS (dashed curve in Figure 6), the ratio decreases for the conductive anomaly model.

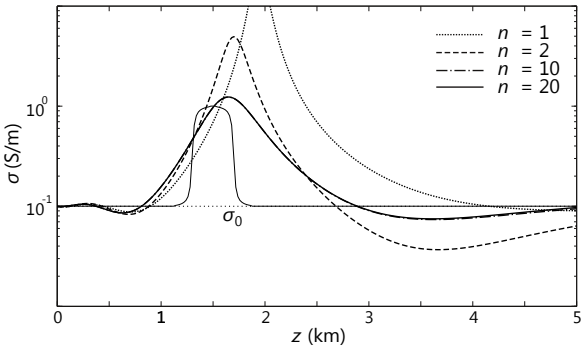

Figure 13. MISS solutions for the conductive anomaly model shown in Figure 4. The solutions are derived from equation (39) and compared for increasing order n of the inverse series. The thin solid curve denotes the true model. Contrary to the ISS (Figure 5), the MISS converges.

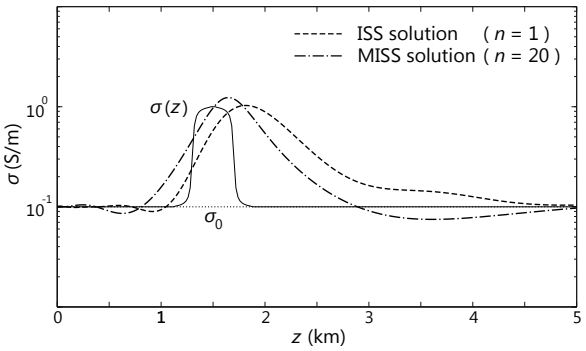

Figure 14. Comparison between the reconstructed models from the ISS and MISS for the conductive anomaly model shown in Figure 4. The MISS solution (dot-dashed curve) is closer to the true model (thin solid curve) than the model reconstructed by the Born approximation of the ISS (dashed curve).

obvious near the resistive target. This difference originates from the fact that the relatively conductive background medium shields the resistive structure, and the reconstruction of the resistive target is physically limited. As a result, the inverse problem is ill-posed, and the solutions shown in Figure 11 are constrained by the employed regularization. Since the regularization acts on different functions in the ISS and MISS (M and R, respectively) with different regularization parameters, the reconstructed models differ. With respect to the location and conductivity value of the reconstructed resistive structure, the MISS yields a model that is closer to the true model (solid curve) than the ISS. From equations (21) and (39), we can express the differential dependence of the electric conductivity on the two parameters M and R as

$$\frac{\partial \sigma}{\partial M} = \sigma_0 e^M = \sigma \tag{41}$$

and

$$\frac{\partial \sigma}{\partial R} = \frac{2\sigma_0}{(1-R)^2} = \frac{(\sigma+\sigma_0)^2}{2\sigma_0}, \tag{42}$$

respectively, where M and R are the partial sums up to the nth order. These equations suggest that the variation of the electric conductivity depends more strongly on the conductivity ratio R than on the logarithm of the conductivity M:

$$\frac{\partial \sigma}{\partial M} < \frac{\partial \sigma}{\partial R}\,. \tag{43}$$

As depicted in Figure 11, the MISS therefore enables more detailed model reconstruction than the ISS.

5.2 Conductive anomaly model

Figures 4 and 5 illustrate that the ISS do not converge for the conductive anomaly model. This divergence arises from the fact that the electric conductivity from the Born approximation surpasses the approximate limit shown in expression (25), and the left hand side of equation (20), D_n, diverges (dashed curve in Figure 6). The MISS, on the other hand, is based on an absolutely converging forward series and free from the limitation. Figure 12 illustrates that for the same conductive anomaly model, the left hand side of equation (38), $\tilde{D}_n$, decreases. The MISS thus yields a solution that corresponds to the prediction of the convergence criterion in Figure 4(b) ($|G^s/G_0| < 1$). Figure 13 shows that contrary to the ISS, the MISS converges to a model that reveals the conductive anomaly structure. The convergence of the MISS demonstrates that it provides a converging solution for a larger contrast between the true and reference models than the ISS. Figure 14 compares the reconstructed model from the MISS with that from the Born approximation of the ISS. As in the case of the resistive anomaly model, the MISS solution is

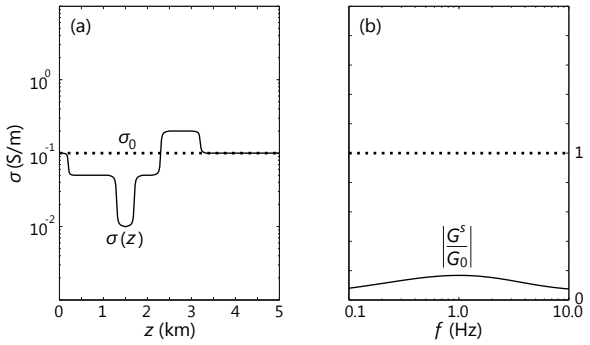

Figure 15. Complex anomaly model. (a) True model (solid curve) versus reference model (dotted line) of the inverse series. The reference conductivity is identical with the background conductivity of the true model. (b) The convergence requirement of the inverse series, expression (16), is satisfied in the employed frequency range.

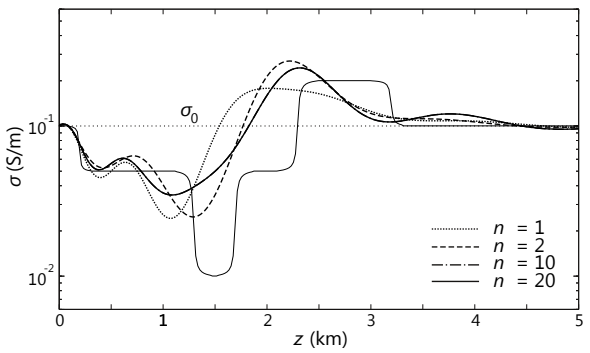

Figure 16. ISS solutions for the complex anomaly model shown in Figure 15. The solutions are derived from equation (21) and compared for increasing order n of the inverse series. The thin solid curve denotes the true model. The ISS converges.

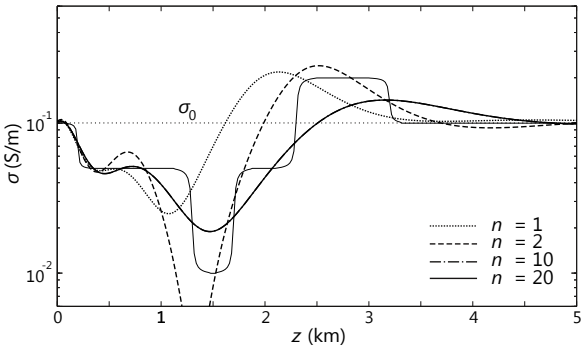

Figure 17. MISS solutions for the complex anomaly model shown in Figure 15. The solutions are derived from equation (39) and compared for increasing order n of the inverse series. The thin solid curve denotes the true model. Both the ISS (Figure 16) and MISS converge.

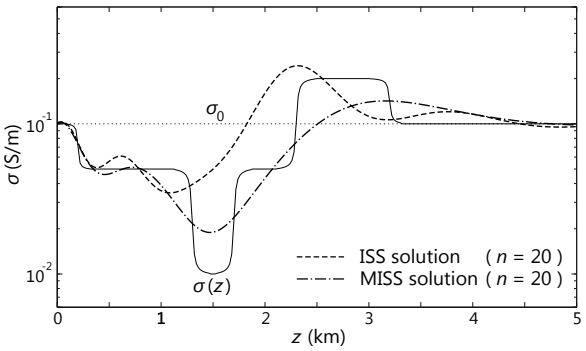

Figure 18. Comparison between the reconstructed models from the ISS and MISS for the complex anomaly model shown in Figure 15. The true (thin solid curve) and reference (dotted line) models are also depicted. The ISS does not retrieve the resistive structure at z = 1.3 - 1.7 km. The MISS, on the other hand, recovers the resistive structure.

closer to the conductive target than the model retrieved via the ISS.

5.3 Complex anomaly model

We consider a complicated conductivity structure that further highlights the advantage of the modified approach over the ISS. Figure 15(a) shows the true and reference conductivity distributions of the complex anomaly model, and Figure 15(b) depicts the ratio between the scattered field and reference Green function. Within the employed frequency range, the scattered field satisfies the convergence criterion of the inverse series in expression (16), and both the ISS and MISS converge (Figures 16 and 17). Compared to the previous models, the contribution of the higher order terms in the inverse series is more pronounced for the complex anomaly model. As a result, the solutions evaluated up to the 20th order are substantially different from the models reconstructed by the Born approximation, which suggests that the ISS and MISS are more significant with increasing model complexity. This reflects that the Born approximation cannot be expected to give a useful result for strongly non-linear problems (Snieder, 1990).

Figure 18 compares the reconstructed models from the ISS and MISS. The difference between the two solutions is insignificant near the source/receiver location (z = 0) but increases with distance from that location. Note that the MISS recovers the resistive structure at z = 1.3 - 1.7 km, which the ISS fails to retrieve. This example demonstrates that compared to the ISS, the modified approach more effectively reconstructs the complicated conductivity structure. Combined with the previous model test that demonstrates the robust convergence of the MISS, the successful reconstruction of the complex anomaly structure manifests the superiority of the modified approach to the original.

6 CONCLUSIONS

We formulated the ISS and MISS for the 1D electromagnetic radiation geometry and identified the difference between the convergence patterns of the two approaches for three representative anomaly structures: the resistive, conductive, and complex anomaly models. We also studied the difference between the reconstructed models from the ISS and MISS. The analysis of the ISS shows that in addition to the convergence condition of the inverse series, there is another condition that determines the convergence/divergence of the ISS, and this condition is closely related to the convergence condition of the forward series. These two convergence conditions are contradictory and, as a result, strongly restrict the application of the ISS: the inverse series converges only for a narrow range of a reference conductivity that is close enough to a true model. The MISS, on the other hand, allows one to more freely choose a reference model, and the newly identified convergence condition no longer affects the convergence of the MISS. Moreover, the models reconstructed by the MISS are closer to the true models than the models generated via the ISS: the resistive target of the complex anomaly model is not identified by the ISS while the modified approach retrieves the target within the resolution limits of the inverse problem. In addition to the robust convergence, the estimate of the resistive target signifies that the MISS is more advantageous than the ISS for the reconstruction of electric conductivity, which varies in the order of magnitude within the subsurface.

The Born approximation plays the most significant role during the iterative model update of the inverse series. The contribution of the higher order terms are insignificant for the simple structures with an isolated resistive or conductive anomaly. The higher order terms, however, play a more significant role in the inversion with increasing model complexity: in the case of the complex anomaly model, the solution evaluated up to the 20th order of the MISS is substantially different from the model retrieved from the Born approximation. In searching for a hydrocarbon reservoir, the electromagnetic inversion involves complex geological structures and is a computationally intensive process. The MISS is therefore an effective scheme that can provide a good starting model for more rigorous large-scale inversion for the three-dimensional conductivity structure of the subsurface. In this study, we consider the 1D radiation geometry shown in Figure 1, assume that the source and receiver are coincident, and simplify the left hand side of equations (20) and (38) as equations (15) and (37), respectively. However, the application of the MISS to more general cases is straightforward, and the conclusions deduced in this study are still valid for 3D radiation geometries and arbitrary source/receiver locations.

7 ACKNOWLEDGEMENTS

This work was supported by the Consortium Project on Seismic Inverse Methods for Complex Structures at Center for Wave Phenomena (CWP). We acknowledge Arthur Weglein (University of Houston), Dmitry Avdeev (Halliburton), and Yuanzhong Fan (Shell International) for helpful information, discussions, and suggestions. We are also grateful to colleagues of CWP for valuable discussions and technical help.

REFERENCES

Abubakar, A., Li, M., Liu, J., & Habashy, T. M., 2009, Simultaneous joint inversion of MT and CSEM data using a multiplicative cost function: *SEG Expanded Abstract*, **28**, 719 – 723.

Alumbaugh, D. L., Newman, G. A., Prevost, L., & Shadid, J. N., 1996, Three-dimensional wideband electromagnetic modeling on massively parallel computers: *Radio Science*, **31**, 1 – 23.

Avdeev, D. B., Kuvshinov, A. V., Pankratov, O. V., & Newman, G. A., 1997, High-performance three-dimensional electromagnetic modelling using modified Neumann series. Wide-band numerical solution and examples: *Journal of Geomagnetism and Geoelectricity*, **49**, 1519 – 1539.

Avdeev, D. B., Kuvshinov, A. V., Pankratov, O. V., & Newman, G. A., 2002, Three-dimensional induction logging problems, Part I: An integral equation solution and model comparisons: *Geophysics*, **67**, 413 – 426.

Avdeev, D. B., 2005, Three-dimensional electromagnetic modelling and inversion from theory to application: *Surveys in Geophysics*, **26**, 767 – 799.

Berenger, J. P., 1994, A perfectly matched layer for the absorption of electromagnetic waves: *Journal of Computational Physics*, **114**, 185 – 200.

Chave, A., & Cox, C. S., 1982, Controlled electromagnetic sources for measuring electrical conductivity beneath the oceans 1. Forward problem and model study: *Journal of Geophysical Research*, **87**, 5327 – 5338.

Colton, D., & Kress, R., 1998, *Inverse acoustic and electromagnetic scattering theory*, 2nd Edition. Springer.

Commer, M., & Newman, G. A., 2008, New advances in three-dimensional controlled-source electromagnetic inversion: *Geophysical Journal International*, **172**, 513 – 535.

Commer, M., & Newman, G. A., 2009, Three-dimensional controlled-source electromagnetic and magnetotelluric joint inversion: *Geophysical Journal International*, **178**, 1305 – 1316.

Constable, S. C., Parker, R. L., & Constable, C. G., 1987, Occam's inversion: A practical algorithm for generating smooth models from electromagnetic sounding data: *Geophysics*, **52**, 289 – 300.

Cox, C. S., Constable, S. C., Chave, A. D., & Webb, S. C., 1986, Controlled-source electromagnetic sounding of the oceanic lithosphere: *Nature*, **320**, 52 – 54.

Gel'fand, I. M., & Levitan, B. M., 1951, On the determination of a differential equation from its spectral function: *Izvestiya Akademii Nauk SSSR Seriya Matematicheskaya*, **15**, 309 – 360.

Golub, G. H., & Reinsch, C., 1970, Singular value decomposition and least squares solutions: *Numerische Mathematik*, **14**, 403 – 420.

Habashy, T. M., Groom, R. W., & Spies, B. R., 1993, Beyond the Born and Rytov approximations: A nonlinear approach to electromagnetic scattering: *Journal of Geophysical Research*, **98**, 1759 – 1775.

Hansen, P. C., 1992, Analysis of discrete ill-posed problems by means of the L-curve: *SIAM Review*, **34**, 561 – 580.

Hohmann, G. W., 1975, Three-dimensional induced polarization and electromagnetic modeling: *Geophysics*, **40**, 309 – 324.

Hoversten, G. M., Cassassuce, F., Gasperikova, E., Newman, G. A., Chen, J., Rubin, Y., Hou, Z., & Vasco, D., 2006, Direct reservoir parameter estimation using joint inversion of marine seismic AVA and CSEM data: *Geophysics*, **71**, C1 – C13.

Hu, W., Abubakar, A., & Habashy, T. M., 2009, Joint electromagnetic and seismic inversion using structural constraints: *Geophysics*, **74**, R99 – R109.

Jackson, D. D., 1972, Interpretation of inaccurate, insufficient and inconsistent data: *Geophysical Journal of the Royal Astronomical Society*, **28**, 97 – 109.

Jackson, J. D., 1999, *Classical electrdynamics*, 3rd Edition. Wiley.

Jost, R., & Kohn, W., 1952, Construction of a potential from a phase shift: *Physical Review*, **87**, 977 – 992.

Kuvshinov, A., Utada, H., Avdeev, D., & Koyama, T., 2005, 3-D modelling and analysis of Dst C-responses in the North Pacific Ocean region, revisited: *Geophysical Journal International*, **160**, 505 – 526.

Kwon, M. J., & Snieder, R., 2010, Comparison between scattering series solutions for acoustic wave and electromagnetic diffusion equations: *SEG Expanded Abstract*, **29**, 758 – 763.

Kwon, M. J., & Snieder, R., 2011, Uncertainty analysis for the integration of seismic and CSEM data: *Geophysical Prospecting*, **59**, doi: 10.1111/j.1365-2478.2010.00937.x.

Lippmann, B. A., & Schwinger, J., 1950, Variational principles for scattering processes. I: *Physical Review*, **79**, 469 – 480.

Morse, P. M., & Feshbach, H., 1953, *Methods of theoretical physics*. McGraw-Hill.

Moses, H. E., 1956, Calculation of the scattering potential from reflection coefficients: *Physical Review*, **102**, 559 – 567.

Newman, G. A., & Alumbaugh, D. L., 1997, Three-dimensional massively parallel electromagnetic inversion - I. Theory: *Geophysical Journal International*, **128**, 345 – 354.

Pankratov, O. V., Avdeev, D. B., & Kuvshinov, A. V., 1995, Electromagnetic field scattering in a heterogeneous earth: A solution to the forward problem: *Physics of the Solid Earth*, **31**, 201 – 209.

Parker, R. L., 1977, Understanding inverse theory: *Annual Review of Earth and Planetary Sciences*, **5**, 35 – 64.

Pridmore, D. F., Hohmann, G. W., Ward, S. H., & Sill, W. R., 1981, An investigation of finite-element modeling for electrical and electromagnetic data in three dimensions: *Geophysics*, **46**, 1009 – 1024.

Prosser, R. T., 1969, Formal solutions of inverse scattering problems: *Journal of Mathematical Physics*, **10**, 1819 – 1822.

Singer, B. S., & Fainberg, E. B., 1995, Generalization of the iterative dissipative method for modeling electromagnetic fields in nonuniform media with displacement current: *Journal of Applied Geophysics*, **34**, 41 – 46.

Singer, B. S., 1995, Method for solution of Maxwell's equations in non-uniform media: *Geophysical Journal International*, **120**, 590 – 598.

Snieder, R., 1990, A perturbative analysis of non-linear inversion: *Geophysical Journal International*, **101**, 545 – 556.

Snieder, R., 1998, The role of nonlinearity in inverse problems: *Inverse Problems*, **14**, 387 – 404.

Srnka, L., Carazzone, J. J., Ephron, M. S., & Eriksen, E. A., 2006, Remote reservoir resistivity mapping: *The Leading Edge*, **25**, 972 – 975.

Tikhonov, A. N., & Arsenin, V. Y., 1977, *Solution of ill-posed problems*. Winston.

Torres-Verdín, C., & Habashy, T. M., 2001, Rapid numerical simulation of axisymmetric single-well induction data using the extended Born approximation: *Radio Science*, **36**, 1287 – 1306.

Um, E. S., Harris J. M., & Alumbaugh D. L., 2010, 3D time-domain electromagnetic diffusion phenomena: A finite-element electric-field approach: *Geophysics*, **75**, F115 – F126.

Weglein, A. B., Gasparotto, F. A., Carvalho, P. M., & Stolt, R. H., 1997, An inverse-scattering series method for attenuating multiples in seismic reflection data: *Geophysics*, **62**, 1975 – 1989.

Weglein, A. B., Araújo, F. V., Carvalho, P. M., Stolt, R. H., Matson, K. H., Coates, R. T., Corrigan, D., Foster, D. J., Shaw, S. A., & Zhang, H., 2003, Inverse scattering series and seismic exploration: *Inverse Problems*, **19**, R27 – R83.

Weglein, A. B., Liu, F., Wang, Z., Li, X., & Liang, H., 2010, The inverse scattering series depth imaging algorithms: development, tests and progress towards field data applications: *SEG Expanded Abstract*, **29**, 4133 – 4138.

Yee, K. S., 1966, Numerical solution of initial boundary value problems involving Maxwell's equations in isotropic media: *IEEE Transactions on Antennas and Propagation*, **14**, 302 – 307.

Zhdanov, M. S., Lee, S. K., & Yoshioka, K., 2006, Integral equation method for 3D modeling of electromagnetic fields in complex structures with inhomogeneous background conductivity: *Geophysics*, **71**, G333 – G345.